RSC Advances

PAPER

Freestanding Co$_3$O$_4$ nanowire array for high performance supercapacitors†

Xin-hui Xia, Jiang-ping Tu,* Yong-qi Zhang, Yong-jin Mai, Xiu-li Wang,* Chang-dong Gu and Xin-bing Zhao

We report a single-crystalline Co$_3$O$_4$ nanowire array grown on a nickel foam prepared by a hydrothermal synthesis method for supercapacitor application. The Co$_3$O$_4$ nanowires show sharp tips and have an average diameter of 70 nm, and a length up to 25 μm. Impressively, the as-prepared single-crystalline Co$_3$O$_4$ nanowire array exhibits noticeable pseudocapacitive performance with a high capacitance of 754 F g^{-1} at 2 A g^{-1} and 610 F g^{-1} at 40 A g^{-1} as well as excellent cycling stability. The enhanced supercapacitor performance is due to the unique one-dimensional (1D) architecture, which provides fast diffusion paths for ions and facilitates the electron and ion transfer on the Co$_3$O$_4$/electrolyte interfaces. Moreover, the 1D nanowire array can accommodate the volume expansion and restrain the pulverization and deterioration of Co$_3$O$_4$ during the repeated cycling process, resulting in enhanced cycling stability.

1. Introduction

High-performance electrochemical energy storage systems are highly desirable in today's information-rich, mobile society.[1] Of the various power sources, supercapacitors represent an emerging energy storage technology that offers fast recharge ability, high power density and long cycle life.[2,3] They have an important role in complementing or replacing batteries in the energy storage field ranging from portable electronics to hybrid electric vehicles. Early studies of supercapacitors mainly focus on electrical double-layer capacitors (EDLCs) based on carbonaceous materials, which suffer from relatively low specific capacitance and instability at a high charge-discharge rate.[4] Such a limited specific capacitance of EDLCs is far from perfect to meet the higher requirements for peak-power assistance in electric vehicles. In recent years, supercapacitors based on pseudocapacitive materials have evoked considerable interest due to their much higher energy density and specific capacitance (several times larger than those of carbonaceous materials) originating from reversible multielectron redox faradaic reactions.[5–8] Among these available pseudocapacitive candidates, Co$_3$O$_4$ is considered to be one of the most attractive materials due to its high specific capacitance (theoretical specific capacitance up to 3560 F g^{-1}), good capability retention and high redox reactivity.[9]

Despite high capacitance, pseudocapacitive materials often present a compromise between the power performance and reversibility due to the slow kinetics of ion and electron transport in electrodes and at the electrode/electrolyte interface. In order to enhance the redox kinetics, great efforts have been devoted to creating porous nanostructured materials with large surface area and short diffusion path of ions and electrons to improve the utilization of pseudocapacitive materials at high power density.[10] Recently, one-dimensional (1D) array architecture (nanorods, nanotubes and nanowires, *etc.*) built on conductive substrates has been demonstrated to be an optimized architecture for boosting the pseudocapacitive performance since single nanowire/nanorod directly contacting with current collector can serve as a superhighway for fast ion and electron transport, resulting in reduced internal resistance and improved high-power performance.[11–15] To date, 1D Co$_3$O$_4$ arrays such as nanotubes, nanowires and nanoneedles have been synthesized by using porous alumina,[16] ammonia-evaporation induction,[17,18] virus as templates,[19] hydrothermal synthesis method,[20] and their enhanced electrochemical performance for lithium ion batteries have been demonstrated. However, there are only a few reports about self-supporting 1D Co$_3$O$_4$ arrays for supercapacitor applications. Previously, Gao *et al.*[21] reported a Co$_3$O$_4$ nanowire array prepared by an ammonia-evaporation induction method for supercapacitor application. Despite its high capacity of 746 F g^{-1}, the cycling stability and high-rate performances are far from satisfactory. The Co$_3$O$_4$ nanowire array obtained by Gao *et al.*[21] exhibited poor cycling stability with 14% capacitance loss after 500 cycles at a current density of 10 mA cm^{-2} (corresponding to a current density of 0.6 A g^{-1}). Besides, our group reported a self-supported hollow Co$_3$O$_4$ nanowire array with oxygen induction and investigated its pseudocapacitive performance.[22] In the present work, we present a single-crystalline Co$_3$O$_4$ nanowire array *via* a facile hydrothermal method and apply it as cathode material for supercapacitors. Impressively, the single-crystalline Co$_3$O$_4$ nanowire array exhibits noticeable pseudocapacitive performance with high capacitance of 754 F g^{-1} at 2 A g^{-1} and 610 F g^{-1} at 40 A g^{-1} as well as excellent cycling stability.

State Key Laboratory of Silicon Materials and Department of Materials Science and Engineering, Zhejiang University, Hangzhou, 310027, China. E-mail: tujp@zju.edu.cn; wangxl@zju.edu.cn; Fax: +(86)-571-87952856; Tel: +(86)-571-87952573

2. Experimental

2.1 Chemical materials

All solvents and chemicals were of reagent quality and were used without further purification. The cobalt nitrate, ammonium fluoride and urea were obtained from Shanghai Chemical Reagent Co. All aqueous solutions were freshly prepared with high purity water (18 MΩ cm resistance).

2.2 Preparation of self-supported single-crystalline Co_3O_4 nanowire array

In a typical synthesis, 10 mmol of $Co(NO_3)_2$, 20 mmol NH_4F and 50 mmol of $CO(NH_2)_2$ were dissolved in 70 mL of distilled water to form homogeneous solution. Then the homogeneous solution prepared above was transferred into Teflon-lined stainless steel autoclave liners. After that, a piece of clean nickel foam substrate with 3×7 cm^2 in size was immersed into the reaction solution. Its top side was protected for solution contamination by uniformly coating with a polytetrafluoroethylene tape. The liner was sealed in a stainless steel autoclave, maintained at 120 °C for 9 h, and then allowed to cool to room temperature naturally. Then, the precursor was collected and rinsed with distilled water several times in order to remove the free particle debris and the residual reactant. Finally, the precursor was annealed at 350 °C in argon for 2 h leading to the formation of Co_3O_4. The load weight of Co_3O_4 is about 4.5 mg cm^{-2}.

2.3 Characterization

The precursor powder was analyzed by thermogravimetry (TG) and differential thermal analysis (DTA) under N_2 atmosphere at a heating rate of 10 °C min^{-1} in a temperature range of 50–600 °C. The morphologies and structures of samples were characterized by X-ray diffraction (XRD, RIGAKU D/Max-2550 with Cu-Kα radiation), field emission scanning electron microscopy (FESEM, FEI SIRION), high-resolution transmission electron microscopy (HRTEM, JEOL JEM-2010F) and fourier transform infrared (FTIR) measurements (Perkin Elmer System 2000 FTIR interferometer).

The electrochemical measurements were carried out in a three-electrode electrochemical cell containing 2 M KOH aqueous solution as the electrolyte. Cyclic voltammetry (CV) measurements were performed on a CHI660c electrochemical workstation (Chenhua, Shanghai). CV measurements were carried out at different scanning rates between 0 V and 0.75 V at 25 °C, Co_3O_4 nanowire array as the working electrode, Hg/HgO as the reference electrode and a Pt foil as the counter-electrode. The galvanostatic charge–discharge tests were conducted on a LAND battery program-control test system. The Co_3O_4 electrodes, together with a nickel mesh counter electrode and an Hg/HgO reference electrode were tested in a three-compartment system. The specific capacitance was calculated according to the following equation:

$$C = \frac{I\Delta t}{M\Delta V} \qquad (1)$$

where C (F g^{-1}) was the specific capacitance, I (mA) represented the discharge current, and M (mg), $\Delta V(v)$ and Δt (sec)

designated the mass of active materials, potential drop during discharge and total discharge time, respectively. Energy density (E) was derived from the following equation:

$$E = \frac{1}{2}C\Delta V^2 \qquad (2)$$

where C was the specific capacitance of the active material, and ΔV was the voltage across the electrode. The power density (P) was calculated from the following equation:

$$P = \frac{E}{\Delta t} \qquad (3)$$

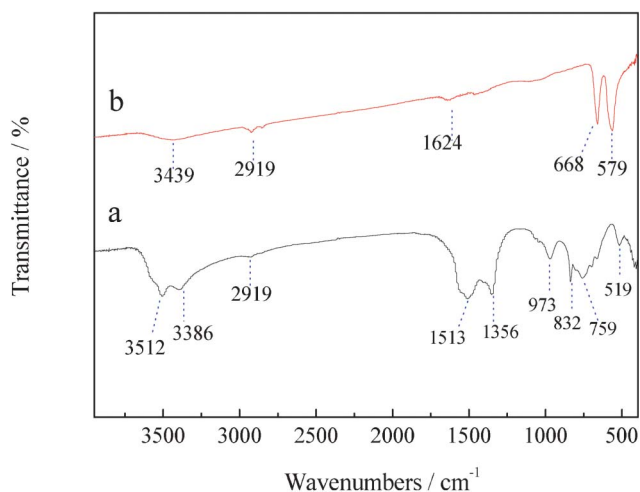where E was the energy density, and Δt was the discharge time.

3. Results and discussion

3.1 Synthesis and characterization of single-crystalline Co_3O_4 nanowire arrays

Self-supported Co_3O_4 nanowire arrays grown on nickel foam are synthesized by a facile hydrothermal method in combination with heat treatment. Fig. 1 shows the XRD patterns of the precursor film and the final product. All the reflection peaks of the precursor film could be well indexed to crystalline orthorhombic basic cobalt carbonate hydroxide $Co_2(OH)_2(CO_3)$ (JCPDS 48-0083) (Fig. 1a). After heat treatment, all the diffraction peaks are attributed to spinel Co_3O_4 phase (JCPDS 42-1467), indicating that the crystalline Co_3O_4 has been formed after annealing treatment (Fig. 1b), supported by the color change of the product from the original pink to black (Fig. S1, ESI†). Meanwhile, thermogravimetric analysis (Fig. S2, ESI†) reveals that 23 wt.% of mass loss is also consistent with the calculated value from basic cobalt carbonate hydroxide $Co_2(OH)_2(CO_3)$ to Co_3O_4. The formation of Co_3O_4 is also verified by the FTIR result (Fig. 2). Excepting for the stretching vibrations of νO–H (3512 cm^{-1} and 3386 cm^{-1}), the $Co_2(OH)_2(CO_3)$ precursor film contains stretching vibrations of νOCO_2 (1513 cm^{-1}) and νCO_3^{2-} (1356 cm^{-1}, 832 cm^{-1} and 759 cm^{-1}) as well as vibration bands of νCo–O (519 cm^{-1}) and νCo–OH (973 cm^{-1}). The CO_3^{2-} groups are the products of urea hydrolysis. The band at 1624 cm^{-1} corresponds to the angular

Fig. 1 XRD patterns of (a) $Co_2(OH)_2(CO_3)_2$ precursor film and (b) Co_3O_4 nanowire array.

Fig. 2 FTIR spectra of (a) $Co_2(OH)_2(CO_3)_2$ precursor film and (b) Co_3O_4 nanowire array.

deformation of molecular water. The small band around 2919 cm^{-1} comes from the stretching vibration of νC–H. After annealing treatment, the bands of the $Co_2(OH)_2(CO_3)_2$ precursor film disappear and two very strong peaks centered at 668 and 579 cm^{-1} characteristic of spinel Co_3O_4 are noticed, which are consistent with the XRD result.
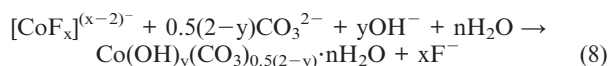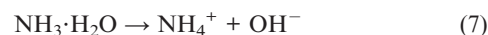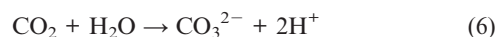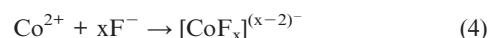
SEM images of the $Co_2(OH)_2(CO_3)_2$ precursor and Co_3O_4 films are presented in Fig. 3. The $Co_2(OH)_2(CO_3)_2$ precursor film shows 1D nanowire arrays architecture (Fig. 3a and b). Apparently, the skeletons of nickel foam are uniformly covered by the nanowires, which grow densely and almost vertically to the substrate. The morphology of the sample before and after annealing treatment does not change much, maintaining the nanowire array structure. The Co_3O_4 nanowires show sharp tips and have an average diameter of 70 nm, length up to around 25 μm (Fig. 3c and d). The length of nanowires could be easily controlled by the growth time.

The structural characterization of an individual nanowire is performed in detail by TEM and HREM observation. The basic cobalt carbonate hydroxide $Co_2(OH)_2(CO_3)_2$ nanowire shows a smooth texture and single crystalline feature (Fig. 4a and b). According to the pattern of selected area electronic diffraction (SAED), the basic cobalt carbonate hydroxide $Co_2(OH)_2(CO_3)_2$ nanowire exhibits a growth direction along [010]. Typical TEM images confirm that the average diameter of an individual Co_3O_4 nanowire is about 70 nm (Fig. 4c and d). The Co_3O_4 nanowire consists of numerous interconnected nanoparticles and presents a rough appearance with a large quantity of mesoporous structures, which is ascribed to the successive release and loss of CO_2 and H_2O during the thermal decomposition of $Co_2(OH)_2(CO_3)_2$ precursor. SAED pattern of a Co_3O_4 nanowire shows a single-crystalline pattern. Three sets of diffraction spots are indexed as (111), (220) and (311) planes of Co_3O_4, respectively. It is noticed that the long axis of the nanowire is parallel to the line that contains both (000) and (220) spots in the SAED pattern, indicating the single-crystalline Co_3O_4 nanowire grows along the [110] direction, similar to those reported by Du et al.,[23] and Xie et al.,[24] and different from those thermal-oxidized Co_3O_4 nanowire with [111] preferential growth.[25]

Fig. 3 Typical SEM images of (a), (b) $Co_2(OH)_2(CO_3)_2$ precursor film and (c), (d) Co_3O_4 nanowire array grown on nickel foam (side view of the arrays and magnified top view presented in insets).

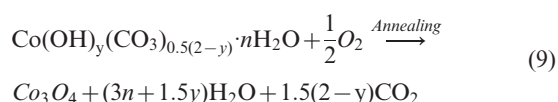Fig. 4e shows a HRTEM image of the side of a Co_3O_4 nanowire. The lattice fringes with a lattice spacing of about 2.42 Å nm corresponds to the (311) planes of Co_3O_4, also revealing that the nanowire is crystalline. Taking the above results together, a plausible growth mechanism of single-crystalline Co_3O_4 nanowires arrays is given as follows.[20]

$$Co^{2+} + xF^- \rightarrow [CoF_x]^{(x-2)-} \quad (4)$$

$$H_2NCONH_2 + H_2O \rightarrow 2NH_3 + CO_2 \quad (5)$$

$$CO_2 + H_2O \rightarrow CO_3^{2-} + 2H^+ \quad (6)$$

$$NH_3 \cdot H_2O \rightarrow NH_4^+ + OH^- \quad (7)$$

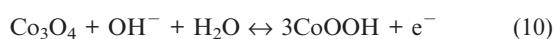$$[CoF_x]^{(x-2)-} + 0.5(2-y)CO_3^{2-} + yOH^- + nH_2O \rightarrow Co(OH)_y(CO_3)_{0.5(2-y)} \cdot nH_2O + xF^- \quad (8)$$

Fig. 4 TEM images of (a), (b) the $Co_2(OH)_2(CO_3)_2$ nanowire and (c), (d) Co_3O_4 nanowire; (e) HRTEM image (SAED patterns of the nanowires presented in inset).

$$Co(OH)_y(CO_3)_{0.5(2-y)} \cdot nH_2O + \frac{1}{2}O_2 \xrightarrow{Annealing}$$
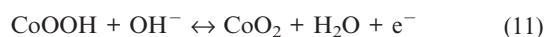$$Co_3O_4 + (3n + 1.5y)H_2O + 1.5(2-y)CO_2 \quad (9)$$

3.2 Electrochemical analysis

The pseudocapacitive behavior of the single-crystalline Co_3O_4 nanowire array was elucidated by cyclic voltammograms (CV) measurements. For Co_3O_4 materials, it is well accepted that their pseudocapacitive process is associated with two redox couples, which are reflected in the CV curve. Two typical redox couples characteristic of Co_3O_4 are observed in the CV curve (Fig. 5a), similar to those reported in the literature.[25,26] The first redox couple A_1/C_1 corresponds to the conversion between CoOOH and Co_3O_4 as illustrated as follows:[21,22]

$$Co_3O_4 + OH^- + H_2O \leftrightarrow 3CoOOH + e^- \quad (10)$$

The second redox couple A_2/C_2 is attributed to the change between CoOOH and CoO_2, represented by the following reaction:[21,22]

$$CoOOH + OH^- \leftrightarrow CoO_2 + H_2O + e^- \quad (11)$$

Note that the nickel foam shows a redox process P1/P2 with low current intensities. This redox couple is attributed to the reversible reaction of Ni(II)/Ni(III) formed on the nickel surface. Compared to Co_3O_4 nanowires array, the signal of nickel foam is quite small, indicating that the nickel foam contribute little to the capacitance of the Co_3O_4 nanowires array. The CV behavior of the Co_3O_4 nanowire array changes much as the scanning rate increases (Fig. 5b). The oxidation and reduction peaks shift continuously to higher and lower potentials respectively, leading to a larger potential separation between the oxidation and the reduction peak. Furthermore, two oxidation (A_1 and A_2) and reduction peaks (C_1 and C_2) merges with each other leaving one oxidation and reduction peaks at a scanning rate of 200 mV s^{-1}, respectively. The pseudocapacitor properties are

Fig. 5 (a) CV curves of the Co_3O_4 nanowire array and nickel foam in the potential region of 0−0.6 V at a scanning rate of 5 mV s^{-1} at the 10th cycle; (b) CV curves of the Co_3O_4 nanowire array at different scanning rates; (c) discharge curves of the Co_3O_4 nanowire array at different discharge current densities after activation for 1000 cycles at 2 A g^{-1} and (d) corresponding specific capacitance at different discharge current densities; (e) Ragone plot (power density vs. energy density) of the single-crystalline Co_3O_4 nanowire array.

tested by galvanostatic charge–discharge at different current densities. In our case, the Co_3O_4 nanowire array takes approximately 1000 cycles to activate and then delivers the highest capacitance, indicating that the Co_3O_4 nanowire array needs long cycles to activate its potential capacitance. Before activation, the Co_3O_4 nanowire array exhibits pseudocapacitances with 323 F g^{-1} at 2 A g^{-1}, 309 F g^{-1} at 4 A g^{-1}, 290F g^{-1} at 10 A g^{-1}, 272 F g^{-1} at 20 A g^{-1}, 248 F g^{-1} at 40 A g^{-1}, respectively (Fig. S3, ESI†). After activation for 1000 cycles at 2 A g^{-1}, the discharge specific capacitances at various current densities increase greatly with 754 F g^{-1} at 2 A g^{-1}, 727 F g^{-1} at 4 A g^{-1}, 689 F g^{-1} at 10 A g^{-1}, 647 F g^{-1} at 20 A g^{-1}, 610 F g^{-1} at 40 A g^{-1}, respectively (Fig. 5c and d), maintaining 81% of capacitance when the charge–discharge rate changes from 2 A g^{-1} to 40 A g^{-1}. In our case, the increase in capacitance is quite large due to the subsequent activation of Co_3O_4 nanowires. As we know, a key advantage of supercapacitors is their fast

recharge capability from a few seconds to several minutes. The charge–discharge process is so fast that the active Co_3O_4 could not completely convert to other active phases, resulting in low utilization and low capacitances. In other words, only a fraction of the material is active during the first cycles, while the other material is not activated. As the electrolyte gradually penetrates into the inside of the Co_3O_4 nanowire, more and more part of the nanowire becomes activated and contributes to the increase of capacitance. These obtained values are higher than our previous self-supported hollow Co_3O_4 nanowire arrays (599 F g^{-1} at 2 A g^{-1}),[22] and other power forms,[27,28] comparable to those obtained from Co_3O_4 arrays prepared Gao et al. (746 F g^{-1} at 0.3 A g^{-1}),[21] lower than the nanostructured nanoporous Ni/Co_3O_4 films (2200 F g^{-1}) grown by Deng's group,[26] whose superior capacitance arises from its pseudocapacitive material–conductive matrix composite nanostructures.

Fig. 5e shows the Ragone plot (power density *vs.* energy density) of the Co_3O_4 nanowire array grown on the nickel foam. Our single-crystalline Co_3O_4 nanowire array delivers an energy density of $\sim 25.5\ Wh\ kg^{-1}$ at a high power density of $\sim 11\ kW\ kg^{-1}$, superior to other Co_3O_4 powder materials.[27,28] Moreover, the as-prepared Co_3O_4 nanowire array exhibits excellent capacitance retention properties. Increasing up to 1000 cycles, the capacitance keeps stable and shows negligible loss after 4000 cycles (Fig. 6), indicating its long term cycling stability and high power capability. The cycling characteristic is much better than Co_3O_4 arrays prepared by Gao *et al.*,[21] which exhibits poor cycling stability with 14% capacitance loss after 500 cycles at a current density of 0.6 A g^{-1}. The enhanced pseudocapacitive performance is ascribed to the following morphological benefits: (1) The Co_3O_4 nanowire array directly grown the nickel foam provides good electrical contacts for each nanowire and ensures every nanowire participating in the electrochemical reaction. (2) The open geometry between nanowires allows easier electrolyte penetration to into the inner region of the electrode, in which nanowires are highly exposed and accessible by electrolyte, resulting in reduced internal resistance and faster kinetics. (3) It eliminates the need for binder and conducting additive, which adds extra contact resistance and supplementary, undesirable interfaces. (4) The high surface area of the nanowire array favors the efficient contact between active materials and electrolytes, providing more active sites for electrochemical reactions. (5) The nanowire array structure helps to alleviate the structure damage caused by volume expansion during the cycling process and keep the morphology stable. This feature is particularly helpful for high rate applications, resulting in better cycling performance. The basic morphology of the single-crystalline Co_3O_4 nanowire array is preserved after 4000 cycles (Fig. 7a and b). A TEM image of the Co_3O_4 nanowire after 4000 cycles shows that the nanowire keeps the structure integrity and maintains the single-crystalline structure made up of numerous interconnected nanoparticles with almost the same crystal orientations (Fig. 7a). It is indicated that the crystalline structure of the nanowire does not change, implying that the
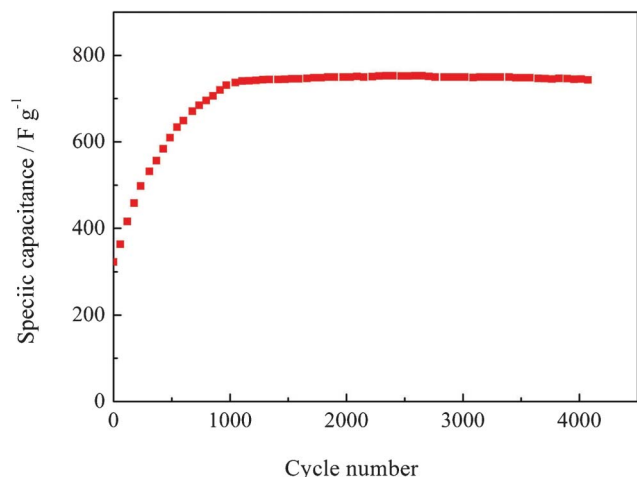

Fig. 7 (a), (b) SEM images of the Co_3O_4 nanowire array after cycling for 4000 cycles; (c) a TEM image of the Co_3O_4 nanowire after cycling for 4000 cycles (SAED pattern in inset).

charge–discharge process mainly happens on the shallow surface.

4. Conclusions

In summary, we have demonstrated a self-supported single-crystalline Co_3O_4 nanowire array grown on the nickel foam as an interesting material for pseudocapacitors with high capacitance, good cyclability and high rate capability. We believe that its outstanding performance comes from the unique porous architecture of the nanowire array. With their ease of fabrication and good performance, this nanowire array will hold promise for application in supercapacitors.

Acknowledgements

Fig. 6 Cycling performance of the Co_3O_4 nanowire array at 2 A g^{-1}.

References

1   A. I. Hochbaum and P. D. Yang, *Chem. Rev.*, 2010, **110**, 527.
2   J. R. Miller and P. Simon, *Science*, 2008, **321**, 651.
3   P. Simon and Y. Gogotsi, *Nat. Mater.*, 2008, **7**, 845.
4   Y. Zhang, H. Feng, X. B. Wu, L. Z. Wang, A. Q. Zhang, T. C. Xia, H. C. Dong, X. F. Li and L. S. Zhang, *Int. J. Hydrogen Energy*, 2009, **34**, 4889.
5   X. D. Li and J. F. Zang, *J. Mater. Chem.*, 2011, **21**, 10965.
6   J. K. Chang, C. M. Wu and I. W. Sun, *J. Mater. Chem.*, 2010, **20**, 3729.
7   Y. Xie, L. Zheng, Y. Xu and D. Jin, *J. Mater. Chem.*, 2010, **20**, 7135.
8   X. H. Xia, J. P. Tu, X. L. Wang, C. D. Gu and X. B. Zhao, *J. Mater. Chem.*, 2011, **21**, 671.
9   X. H. Xia, J. P. Tu, X. L. Wang, C. D. Gu and X. B. Zhao, *Chem. Commun.*, 2011, **47**, 5786.
10 C. Liu, F. Li, L. P. Ma and H. M. Cheng, *Adv. Mater.*, 2010, **22**, E28.
11 Y. Yang, D. Kim, M. Yang and P. Schmuki, *Chem. Commun.*, 2011, **47**, 7746.
12 J. P. Liu, C. W. Cheng, W. W. Zhou, H. X. Li and H. J. Fan, *Chem. Commun.*, 2011, **47**, 3436.
13 R. Liu and S. B. Lee, *J. Am. Chem. Soc.*, 2008, **130**, 2942.
14 R. Liu, J. Duay and S. B. Lee, *ACS Nano*, 2010, **4**, 4299.
15 R. Liu, S. Il Cho and S. B. Lee, *Nanotechnology*, 2008, 19.
16 W. Y. Li, L. N. Xu and J. Chen, *Adv. Funct. Mater.*, 2005, **15**, 851.
17 Y. G. Li, B. Tan and Y. Y. Wu, *J. Am. Chem. Soc.*, 2006, **128**, 14258.
18 Y. G. Li, B. Tan and Y. Y. Wu, *Nano Lett.*, 2008, **8**, 265.
19 K. T. Nam, D. W. Kim, P. J. Yoo, C. Y. Chiang, N. Meethong, P. T. Hammond, Y. M. Chiang and A. M. Belcher, *Science*, 2006, **312**, 885.
20 J. Jiang, J. P. Liu, X. T. Huang, Y. Y. Li, R. M. Ding, X. X. Ji, Y. Y. Hu, Q. B. Chi and Z. H. Zhu, *Cryst. Growth Des.*, 2010, **10**, 70.
21 Y. Y. Gao, S. L. Chen, D. X. Cao, G. L. Wang and J. L. Yin, *J. Power Sources*, 2010, **195**, 1757.
22 X. H. Xia, J. P. Tu, Y. J. Mai, X. L. Wang, C. D. Gu and X. B. Zhao, *J. Mater. Chem.*, 2011, **21**, 9319.
23 J. Du, L. L. Chai, G. M. Wang, K. Li and Y. T. Qian, *Aust. J. Chem.*, 2008, **61**, 153.
24 X. W. Xie, Y. Li, Z. Q. Liu, M. Haruta and W. J. Shen, *Nature*, 2009, **458**, 746.
25 X. W. Lou, D. Deng, J. Y. Lee and L. A. Archer, *J. Mater. Chem.*, 2008, **18**, 4397.
26 M. J. Deng, F. L. Huang, I. W. Sun, W. T. Tsai and J. K. Chang, *Nanotechnology*, 2009, **20**, 175602.
27 J. Li, L. Cui and X. G. Zhang, *J. Appl. Electrochem.*, 2009, **39**, 1871.
28 Y. T. Qian, S. L. Xiong, C. Z. Yuan, M. F. Zhang and B. J. Xi, *Chem.–Eur. J.*, 2009, **15**, 5320.